Avalanches and epidemic models of fracturing in earthquakes

J. Lomnitz-Adler
Instituto de Física, Universidad Nacional Autónoma de México, Apartado Postal 20-364, 01000 México D.F., Mexico

L. Knopoff
Department of Physics and Institute of Geophysics and Planetary Physics, University of California, Los Angeles, California 90024

G. Martínez-Mekler
Instituto de Física, Universidad Nacional Autónoma de México, Apartado Postal 20-364, 01000 México D.F., Mexico

(Received 21 March 1991; revised manuscript received 31 October 1991)

The evolutionary history of elastic materials subjected to the shear stress and the high confining pressures encountered in seismological applications is simulated by a set of avalanche models. Some models exhibit bimodal fracture-size distributions reminiscent of a first-order phase transition, while others have scaling behavior. We argue that this scaling behavior arises as a consequence of the high degree of self-generated roughness. In all models the scaling region broadens as surface roughness is increased. An epidemic growth model, closely related to the avalanche models, is introduced to understand the statistical properties obtained in the simulations. By means of these alternative formulations we interpret the scaling in the size distributions of the avalanche models as a finite-size effect; the system self-organizes, tuning itself to a size-dependent steady state which exhibits an apparent criticality. A value for the scaling exponent, determined from the epidemic model by way of correlated percolation theory, is in good agreement with the numerical result. These problems have relevance to sandpile and earthquake models and to aspects of self-organized criticality.

PACS number(s): 05.20.−y, 05.70.Jk, 46.30.Nz, 91.30.Bi

I. INTRODUCTION

In this paper we are concerned with fracture propagation in a regime relevant to the study of earthquakes. Shallow seismic events occur at depths of 10–50 km, with corresponding pressures of 3–15 kbar. In contrast to typical laboratory experiments, these high pressures eliminate the possibility of generating tensile cracks and favor shear fracture. Repeated fracture and healing on a given surface is now possible, and is in fact observed.

In the following we develop several discrete models for fracture propagation on a two-dimensional fault with healing. Based on rock friction experiments that indicate that the velocity dependence of the friction force is weak [1], we work with a velocity-independent dynamical friction coefficient. This assumption is frequently found in the seismological literature. The growth rules we propose for these fractures are given in terms of a nearest-neighbor algorithm valid in the range of parameters of interest. These rules reproduce the scaling laws of elastic cracks.

Our approach is set in the context of the general problem of the statistical study of irreversible phenomena. We work within two frameworks: (i) the "time-average framework," in which a model for the system is allowed to evolve and statistics are obtained by averaging over long time intervals, and (ii) the "ensemble framework," where a series of fractures are generated on a set of systems that satisfy identical "macroscopic" constraints but differ at the "microscopic" level. Models of type (i) are, for example, the avalanche models of Bak, Tang, and Wiesenfeld [2], Zhang [3], Ito and Matsuzaki [4], Carlson and Langer [5], and Nakanishi [6]. Work along the lines of type (ii) has been previously carried out, among others, by Herrmann and collaborators [7], and Lomnitz-Adler and Lemus-Diaz [8]. In equilibrium statistical physics both approaches are in general interchangeable due to an underlying ergodic hypothesis. In our case, despite the absence of a formal justification, we work with both descriptions. The model used in framework (ii) has been constructed to incorporate the essential features of the avalanche models. Both treatments are complementary and provide a fuller understanding of the dynamics of fracture propagation.

As far as self-organized criticality is concerned, while it can be argued that in the thermodynamic limit none of these system have critical points, for any finite lattice one of the models tunes itself to a state which appears critical.

This paper is organized as follows: In Sec. II we present the necessary elements of the theory of elastic crack propagation, to justify that a two-dimensional, nearest-neighbor approximation is valid for modeling seismic fracture. We introduce a set of avalanche models in Sec. III, and interpret the generated statistics in terms of a nucleation model in Sec. IV. In Sec. V we construct an epidemic growth model that corresponds to the avalanche models under consideration. From the

cluster-size distribution of the epidemic model we obtain in Sec. VI, via correlated percolation theory, the exponent observed for the automaton's avalanche-size distribution. Section VII contains our conclusions and a discussion.

II. FRACTURE-PROPAGATION MODEL

A fracture that is introduced into a prestressed solid induces a redistribution of the stress field. The stress on the fracture surface itself is reduced; beyond the fracture surface and in its plane, stresses are increased, significantly so at short distances from the edge of the crack and less so at longer range (see reviews [9]). The amplitude of the redistributed stress fields depends on the size of the crack and the stress drop on the fractured surface. Hence, a succession of cracks induces fluctuations in the stress field.

We simulate a fault which supports repeated seismic events by two-dimensional-lattice models with nearest-neighbor interactions. The conditions under which the nearest-neighbor approximation is appropriate can be derived as follows. A planar crack in the interior of a stressed elastic solid has a stress on its walls equal to the sliding friction; the difference between the external stress and the friction is the stress drop τ. Because we neglect inertial effects in our problem, we take the friction on the crack wall to be zero. For a thin crack of characteristic length L that terminates abruptly at a smooth edge, the exterior stress increment falls off as $\tau(L/\xi)^{1/2}$ at short distance ξ from the edge. At long range the stress increment falls off as the point-source Green's function, which is ξ^{-d} for a d-dimensional crack. If $(L/\xi)^{1/2} \gg 1$, the incremental energy density outside the crack is proportional to the square of the incremental stress, and falls off at a rate proportional to L/ξ. In the case of a two-dimensional antiplane shear crack in an infinite, elastically homogeneous medium, the exact solution for the stress is [9, 10]

$$\sigma = \tau x/(x^2 - L^2)^{1/2}, \quad x > L \tag{2.1}$$

where L is half of the width of a crack and x is measured from the center; $\xi = x - L$. Thus the incremental energy in a finite interval of distance from the edge varies as $L \ln(\xi_1/\xi_2)$, where ξ_1 and ξ_2 are the outer and inner distances of the interval from the edge.

Since a real elastic material with a finite yield stress cannot support the infinity at the edge implied by the short-range dependence, a slip-weakening zone (sometimes called a plastic, transition, or damage zone) develops over the distance ξ_c, where $\tau(L/2\xi_c)^{1/2} = \sigma_Y$ with σ_Y the yield strength of the material (Fig. 1). The transition zone is a tubular region that surrounds and follows the edge; in the transition zone dense dislocations are formed that are displayed as microfracturing, twinning, development of slip lamellae, etc. Outside the slip-weakening zone we assume the material to be homogeneous and elastic.

To fix the range of validity of a nearest-neighbor model of stress redistribution in a lattice model with lattice constant b, we compute the ratio of the energies per unit length of the crack edge in the regions $0 < \xi < b$ and

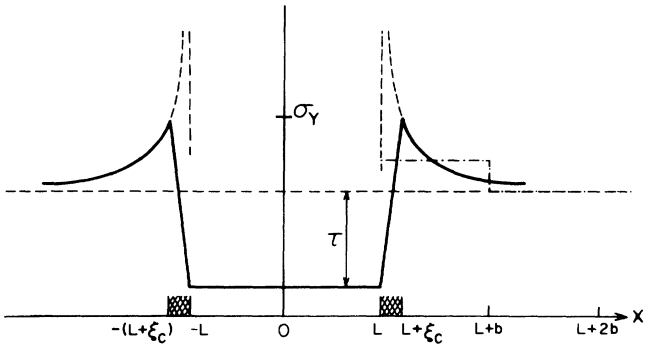

FIG. 1. Distribution of stresses in the plane of fracture (solid curve). The shaded regions denote the slip weakening zone; the lattice spacing b is also indicated. Dotted-dashed curve illustrates the nearest-neighbor approximation.

$b < \xi < 2b$. The energy density is $h = \sigma^2/2\mu$, where μ is the shear modulus. We use the exact expression for a 2D crack given in (2.1). If we assume both a linear stress and a linear shear modulus profile in the slip-weakening zone (see Fig. 1) we obtain, in the limits $(b/L) \ll 1$, $(\xi_c/L) \ll 1$,

$$h_1/h_2 = [\tfrac{1}{2} + \ln(b/\xi_c)]/\ln(2) \; . \tag{2.2}$$

The logarithmic factors describe the energies in the two lattice intervals outside the slip-weakening zone while the first term describes the energy inside it. If the assumptions of the linearity of profiles in the slip-weakening zone are changed, the first factor is changed slightly. Since the stress drop is related to the size of the slip-weakening zone by

$$\tau/\sigma_Y = (2\xi_c/L)^{1/2} \; , \tag{2.3}$$

the nearest-neighbor model will hold in the approximation $\xi_c \ll b$, which implies $\tau/\sigma_Y \ll 1$. Since all dimensions of the redistribution are proportional to the crack size, both for the size of the slip-weakening zone and the decay of the stress outside it, the conditions for the validity of the nearest-neighbor model are fixed by the relations at the largest crack sizes. For a yield stress of 600 bar, and a loading stress of 30 bar, $\tau/\sigma_Y \simeq 0.05$ and the nearest-neighbor approximation fails for fracture dimensions greater than $L/b \simeq 80$. We show below that the physical system loses its mechanical stability long before fractures of this size appear.

III. TIME-AVERAGE FRAMEWORK

We construct several avalanche models that simulate fracture propagation and in which inertial effects are neglected. As a starting point, consider a typical avalanche model recently described in the literature [2,3,4,11]. Space is discretized into a two-dimensional lattice with coordination number z, and at every lattice point (i,j) a scalar variable $h(i,j)$ is defined which we shall refer to as the energy. Time is also discretized, and at every time step one of the lattice sites is chosen at random and a fixed quantity ε is added to it. If the h value

at this point is greater than one, an avalanche is initiated with the following rules: (1) the quantity h/z is transferred to each of the neighbors; (2) h at (i,j) is set to zero (the site breaks); (3) if any of the neighbors has a value of h which is greater than one, the process is repeated until no h exceeds the critical value of one. The "avalanche" occurs during one time step, and in this sense is instantaneous. Once an avalanche has died out, time is increased by one unit and the process described above is repeated.

Features of this model that will be of relevance below are (i) it is locally conservative, unless a site (i,j) is at the edge of the lattice the sum of energies is conserved; (ii) the loading mechanism is random, and over long periods of time builds up an energy surface which approaches a random walk as ε tends to zero; (iii) the avalanche propagates according to a threshold dynamics, i.e., there is a value for h (in this case, one) such that if a site exceeds this value it is unstable; (iv) the algorithm for the dynamics is local in space; (v) external loading is applied over the entire surface, and energy is removed only at the edges. Such a model must be capable of generating avalanches whose dimensions are comparable to the size of the system. This implies [11,12] that in a steady-state regime properties reminiscent of a critical state should be observed. This is the self-organized criticality (SOC) first described by Bak, Tang, and Wiesenfeld [2]; (vi) the dynamics has no memory; a site which has previously transferred its energy to the neighboring sites has exactly the same properties as all of the other lattice sites.

Feature (ii), while being somewhat unrealistic as a tectonic loading mechanism, is a useful prescription to simulate a certain degree of roughness on the fault surface, which, as mentioned before, is subject to repeated healing processes.

Feature (vi) is inappropriate to describe propagating shear cracks; regions that have already broken should not accumulate stress or energy during the fracture event. Therefore we modify rule (1) of the growth algorithm so that once the energy of a site has been reset to zero it cannot accumulate energy for the duration of the avalanche. With this mechanism the concentration of energy at the crack tip increases with L for any two-dimensional crack. For example, consider a circular crack of radius L with average energy per site prior to fracture given by $\langle h \rangle$. The area depleted of energy is $S=\pi L^2$; because of nearest-neighbor interactions, all the energy is transferred to the perimeter whose length is $t=2\pi L$. Hence the average energy per site at the perimeter is

$$\langle h \rangle_{\text{perimeter}} = \langle h \rangle (1+L/2) . \tag{3.1}$$

An identical result is obtained for an infinite two-dimensional crack if L is the half-width of the crack as in (2.1). These statements are consistent with the observation that the stress concentrations scale as $\sqrt{L}$.

The explicit rules of the modified growth algorithm which we study in this paper are as follows.

(1) The quantity h/k is transferred to each of the k neighbors which have not yet participated in the avalanche. Sites which lie outside the lattice boundary are considered to be unbroken.

(2) If $k>0$, $h(i,j)$ is set to zero.

(3) If any of the neighbors has an h value greater than one the process is repeated until no h exceeds the threshold.

In the above algorithm, the case $k=0$, for which the site whose energy exceeds the threshold and has no nearest neighbors to which it can transfer its energy, has not been defined. In Sec. IV three alternative rules will be defined giving rise to three different models.

IV. TIME-AVERAGE BEHAVIOR OF AVALANCHE MODELS

In our numerical simulations it is assumed that the time scale for the fracture (avalanche) is very short compared with the scale for the increase and accumulation of energy. The system was allowed to run for 2×10^7 time steps, in each of which an energy unit of $\varepsilon=\frac{1}{4}$ was added to a site chosen at random. Runs with smaller values of ε were also performed to study the effect of this parameter on the resulting distributions. Prior to taking any statistics, the system evolved for a transient of 10^5 time steps to avoid bias arising from initial conditions. To detect finite-size effects, lattices of 8×8, 16×16, 32×32, and 64×64 sites were studied [in case (3) a 128×128 lattice was also considered]. The fractures were grown in successive shells of sites which broke "simultaneously." We consider three variants of the model which differ for the case $k=0$.

A. Model 1: Local, nonconservative dynamics

The energy at the isolated site is lost to the system and its energy is set to zero. This model is local, in the sense that energy is transferred from one site to its first neighbors, and is nonconservative since the energy at the anomalous site is removed from the plane without redistribution.

The distributions of fracture sizes for model 1 are shown in Fig. 2. As the lattice size increases, the distribution is seen to have two distinct parts. At the small scale there is a large number of small events, which follow an approximate power law over a reduced range of avalanche sizes. At the largest scale there are fractures whose size is essentially equal to the size of the lattice. There are no events in the intermediate range.

The bimodal distribution is reminiscent of two-phase coexistence in a first-order phase transition. A mean-field nucleation argument for the propagation of the avalanche supports this analogy. We define $\langle h \rangle$ as a spatial average taken over the lattice,

$$\langle h \rangle \equiv \sum_{i,j} h_{ij}/N^2 . \tag{4.1}$$

If a circular fracture has a radius

$$L_{\text{tr}} = 2(1-\langle h \rangle)/\langle h \rangle \tag{4.2}$$

(see 3.1), it will grow without bounds because the energy concentration at the perimeter exceeds the fracture threshold. The validity of the assumptions implicit in ex-

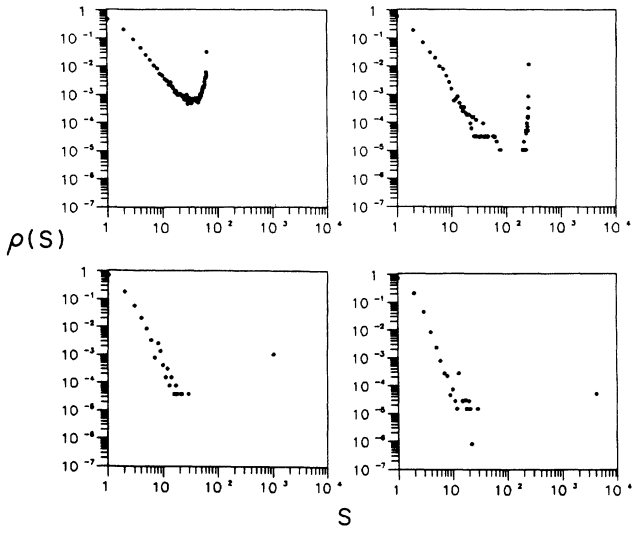

FIG. 2. Avalanche-size distributions of model 1. Lattice sizes range from 8×8 in the upper left-hand corner to 64×64 in the lower right-hand corner.

pression (4.2) can be checked with Fig. 2 and 3. We observe in Fig. 2 that the transition cluster size $S_{tr}=\pi L_{tr}^2$ is of the order of 30, from which L_{tr} is of the order of 3; from (4.2), the corresponding $\langle h \rangle$ is approximately 0.4. Figure 3 shows a histogram for the relative frequency of occurrence of the value of $\langle h \rangle$ over all time steps. Average energies greater than about 0.4 are never encountered, indicating that the largest scale events occur when the energy is close to this value, which we shall refer to as $\langle h \rangle_{tr}$.

As the lattice size increases, the energy histograms of Fig. 3 tend to a boxcar distribution. A one-degree-of-freedom system that has this distribution is a periodic linear sawtooth oscillator. All values of the sawtooth

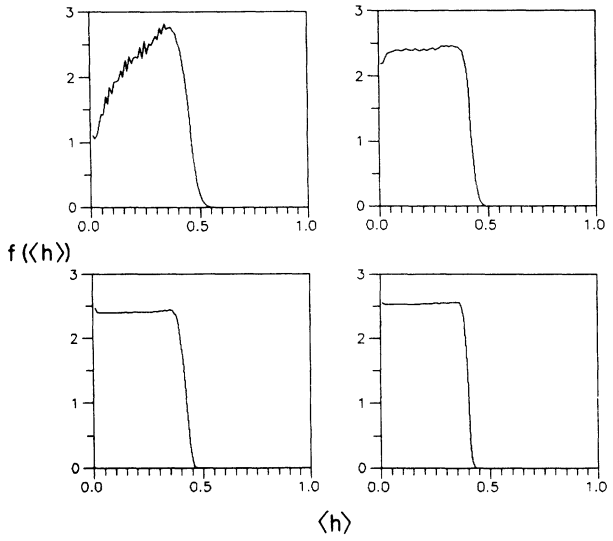

FIG. 3. Relative frequency of occurrence $f(\langle h \rangle)$ of the mean energy $\langle h \rangle$ for model 1.

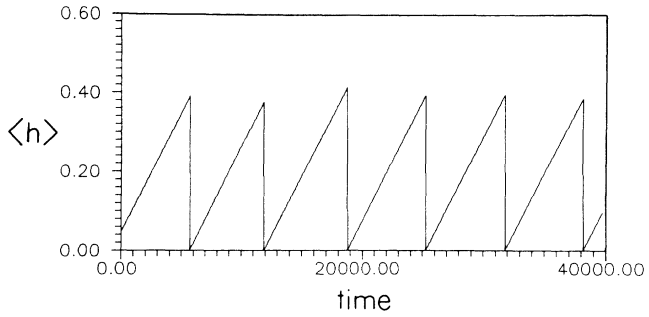

FIG. 4. Time evolution of mean energy $\langle h \rangle(t)$. Note the similarity of this plot with that of a one-dimensional relaxation oscillator.

function between the threshold and the base are sampled with the same probability, while all other states are occupied with probability zero. In Fig. 4 we show that the evolution in time of $\langle h \rangle$ is indeed of this form. Our model has a "charging" period equal to the average time T between two catastrophic events, i.e., avalanches with a size of the order of the system. Under the assumption of small spatial inhomogeneities, a catastrophic event may only occur in the vicinity of the transition energy, which is $H_{MF}=\langle h \rangle_{tr} N^2$ in the mean-field approximation; therefore

$$T=H_{MF}/\varepsilon \ , \tag{4.3}$$

where ε ($=0.25$) is the energy transferred to the system at each time step. We may consider the time-interval distribution between big events, i.e., events whose size is comparable to that of the system. In Fig. 5 we show this distribution for avalanches whose area is larger than or equal to $N^2(1-2/N)$. From (4.3), $T\cong6500$ for the 64×64 lattice.

Since large fractures that leave $h_{ij}=0$ over the entire lattice occur periodically, at no time are there large spatial fluctuations in h. There is a long recovery-time interval of the order of T, during which *no* avalanches occur, as we have observed in the simulations. Thus no events

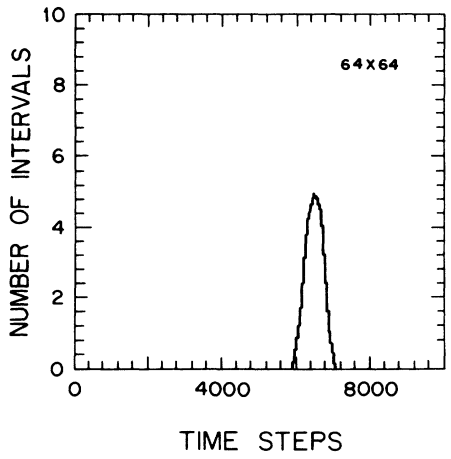

FIG. 5. Distribution of intervals between large events $[S\geq(64)^2(1-\frac{1}{32})]$ for model 1. Lattice size is $(64)^2$.

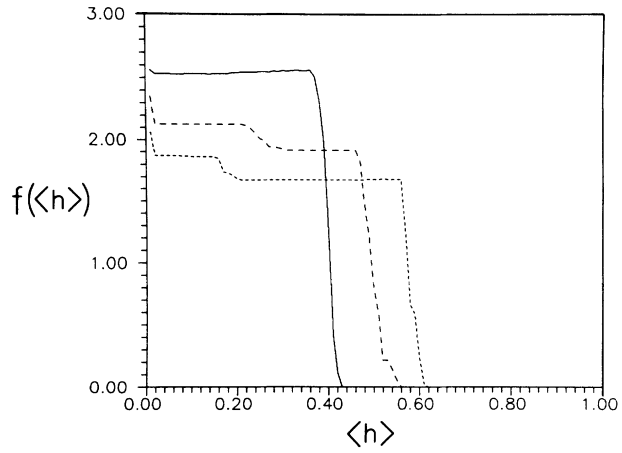

FIG. 6. Variation with ε of the relative frequency of occurrence $f(\langle h \rangle)$ of the mean energy $\langle h \rangle$, in model 1. Solid curve, $\varepsilon=\frac{1}{4}$; dashed curve, $\varepsilon=\frac{1}{8}$; dotted curve, $\varepsilon=\frac{1}{16}$. Note that $\langle h \rangle_{tr}$ decreases with ε.

take place until $\langle h \rangle$ lies just below $\langle h \rangle_{tr}=0.4$. The numerical values of parameters such as $\langle h \rangle_{tr}, L_{tr}$ depend on the level of roughness of the fault surface which is controlled by the parameter ε. Immediately after a large event the energy surface is set to $h_{ij}=0$, and during the charging period, the distribution of energy for any given site is given by the binomial distribution. It follows that for a mean energy $\langle h \rangle$ the width of the energy profile is equal to $\sqrt{\varepsilon \langle h \rangle}$, so that as ε decreases the surface becomes smoother, $\langle h \rangle_{tr}$ increases (see Fig. 6) and L_{tr} decreases (see Fig. 7), qualitative features remaining the same.

As a final remark we point out that in these calculations the nearest-neighbor approximation is valid. The critical cluster length $L_{tr}=3$ is well within the bound $L/b \simeq 80$ obtained in Sec. II.

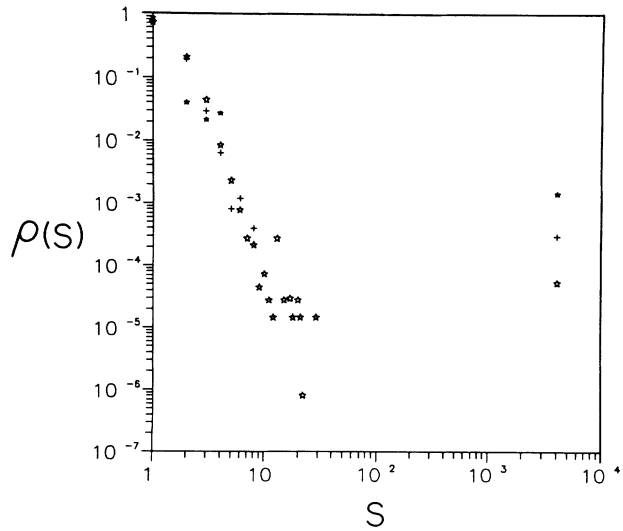

FIG. 7. Variation with ε of the avalanche-size distribution of model 1: open stars, $\varepsilon=\frac{1}{4}$; crosses, $\varepsilon=\frac{1}{8}$; solid stars, $\varepsilon=\frac{1}{16}$. Note how S_{tr} increases with ε.

B. Model 2: Local, conservative, relaxed threshold dynamics

In this model an isolated site with energy greater than the threshold does not break and continues to retain its energy after the fracture has been completed. This site can only break in a future avalanche, which occurs if ε is added to it, or if it is engulfed by a future event initiated elsewhere. This model is inconsistent with a postulate of threshold dynamics, wherein a site that has an energy in excess of a critical threshold is always unstable. We expect to observe large energy variations, especially following a rupture whose size is comparable to that of the entire lattice; at this time most of the sites have $h=0$, but a few sites still can have large values of h. These isolated, highly charged sites can initiate a rupture at any time, and the system can generate avalanches of any size.

Model 2 is conservative, except for fractures which intersect the boundaries of the lattice. It is not a reasonable choice for the modeling of fractures; since the elastodynamic interactions which underlie energy transfers between sites are long range, it is difficult to justify a model in which energy can either be transferred to nearest neighbors or not at all. Our purpose in this exploration is to investigate the role of energy conservation in such models. Although physically unrealistic, the model has some interest from the statistical-mechanics point of view, and shows some generalizable features of collective behavior of extended nonlinear systems that have implications beyond the problems of fracture propagation.

The avalanche-size distribution for this model is shown in Fig. 8. Avalanches of all sizes are present with apparent scale invariance extending up to, but not including, the largest avalanches, where a maximum is once again observed. These simulation results are compatible with the nucleation theory arguments presented in connection with model 1 if the transition avalanche size L_{tr} is of the same order as the lattice length N; in this case,

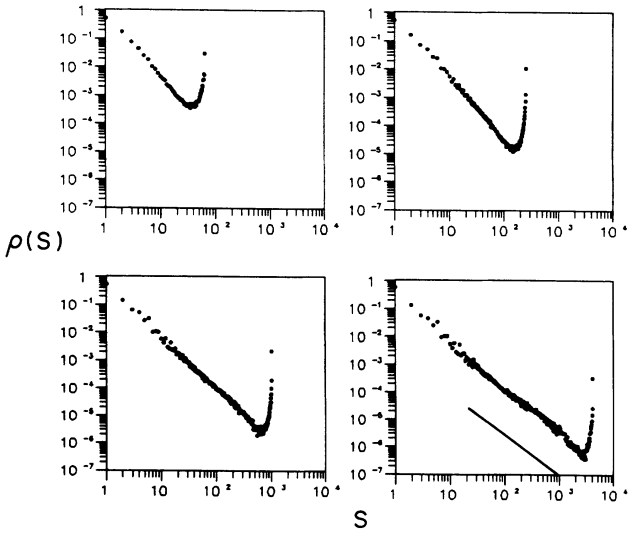

FIG. 8. Avalanche-size distributions of model 2. The solid line has a slope of -1.45.

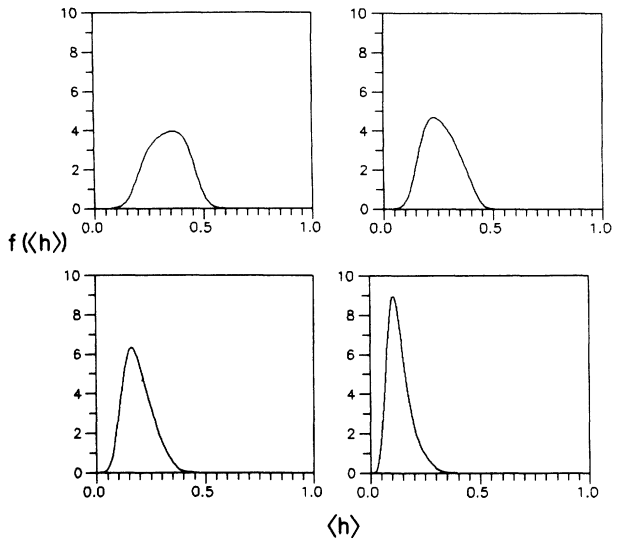

FIG. 9. Relative frequency of occurrence $f(\langle h \rangle)$ of the mean energy $\langle h \rangle$ for model 2.

the average value of $\langle h \rangle$ should scale as $1/N$, from Eq. (4.2).

The distribution of $\langle h \rangle$ becomes sharper as the lattice size is increased, with the maximum shifting to smaller values of $\langle h \rangle$ (Fig. 9). We infer that the system is self-organizing to a steady state. The peak and average values of the distributions scale with N with an exponent that is significantly different from -1.0, namely about -0.5 (Fig. 10), this behavior is an indication that the assumptions behind the nucleation model appropriate for case 1 cannot accommodate case 2 without some modification. If we allow for the possibility of a geometrically complex avalanche boundary, we rewrite Eq. (3.1) as

$$\langle h \rangle_{\text{perimeter}} = \langle h \rangle + \langle h \rangle (S/t) , \tag{4.4}$$

where S is the crack area and t its perimeter. If we assume that t scales with S in terms of an exponent ν defined by

$$t \sim S^{1-\nu} , \tag{4.5}$$

where $\nu \leq 1/2$ is an effective dimension that measures the amount of structure in the perimeter, then $\langle h \rangle$ scales as

$$\langle h \rangle \sim N^{-2\nu} . \tag{4.6}$$

In Fig. 10 we observe that ν is equal to about $\frac{1}{4}$.

With regard to temporal correlations, since large amounts of energy can be accumulated at some sites, small fluctuations in energy can trigger large events at any time. Thus the periodic-relaxation oscillator model is inadequate. In this case large events may be followed by other large events after a short time interval; the time-interval distribution between catastrophic events is not sharply peaked (Fig. 11).

The power-law size distribution over a wide range of fracture sizes (Fig. 8) might lead one to believe that the system is self-organizing into a critical state. There are two objections to this inference: first, the maximum in the avalanche distribution for large fractures is difficult to accommodate in a finite-size scaling treatment of the problem, since the maxima scale with a smaller exponent than the slope in the power-law distribution; second, the maximum in the energy distribution decreases with increasing lattice size, indicating that the "critical state" is size dependent. This latter observation can be understood if the system self-organizes into a steady state such that $L_{\text{tr}} \simeq N$ and if avalanche perimeters are complex. Based on percolation-theory results below, we shall argue that the observed scaling can then be interpreted as a *finite-size effect.*

When the arguments presented above for the scaling of perimeter with fracture size are extended to Eq. (2.3), i.e., $\tau/\sigma_Y \cong (\xi_c/L)^{\nu}$, we find from Eq. (4.6) that the size of

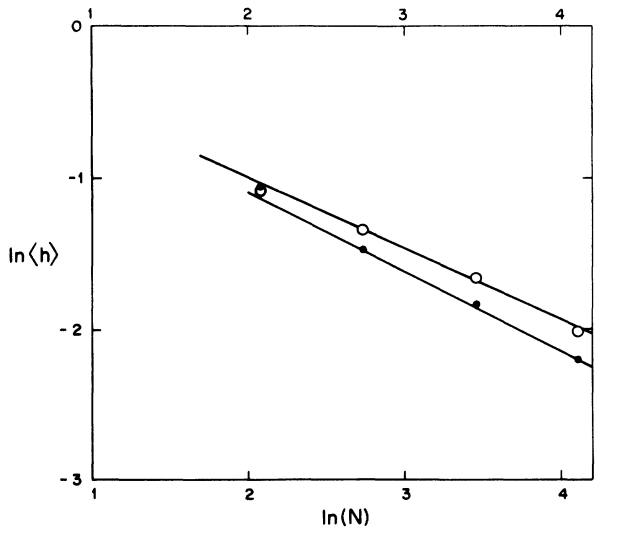

FIG. 10. Scaling of $\langle h \rangle_{\text{MP}}$ with lattice size (model 2). Black dots are the maxima in the distribution of $\langle h \rangle$ (see Fig. 9), whereas white dots are global time averages of $\langle h \rangle$. Straight lines have been drawn to guide the eye and have slopes of -0.51 and -0.47 respectively.

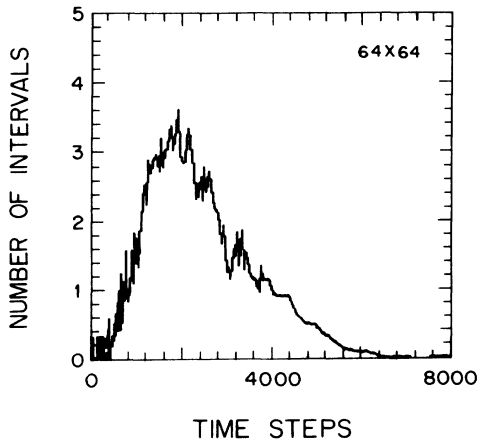

FIG. 11. Distribution of intervals between large events for model 2.

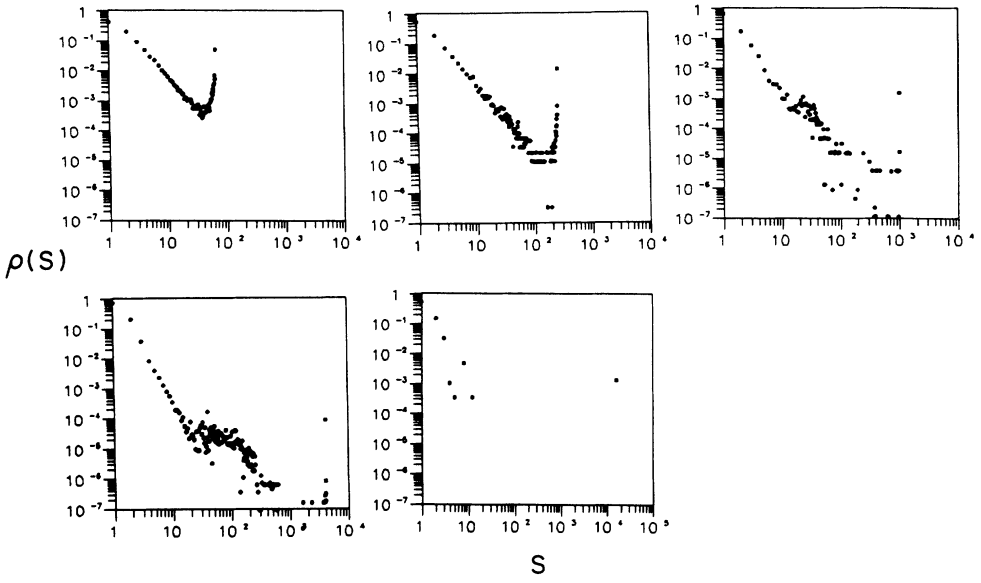

FIG. 12. Avalanche-size distributions of model 3. Largest lattice size is $(128)^2$.

the slip-weakening zone ξ_c of the largest fractures ($L \simeq N$) is independent of the lattice and hence is small.

C. Model 3: Nonlocal, conservative dynamics-implications for self-organized criticality

In this case, the energy of the isolated site is set to zero and is redistributed evenly along the boundary of the broken region. Except for fractures that intersect the boundary of the lattice, this model is also conservative; all energy remains in the fault plane.

The first two models display a radically different phenomenology from one another. In particular, model 2 self-organizes into an apparent critical state. Systems capable of self-organized criticality have attracted a great deal of attention since they were discovered numerically by Bak, Tang, and Wiesenfeld [2], and have been studied in much detail [11,3,12]. Hwa and Kardar [12] have argued that a conservative avalanche model will self-organize critically, while a system that is capable of dissipating energy anywhere besides the lattice boundaries will not. The results from the first two models appear to be consistent with their conclusion. In Hwa and Kardar the analog of the energy was transferred locally. This assumption is important in the arguments on the origin of self-organized criticality given by Kadanoff *et al.* [11]. Our third model is nonlocal and conservative.

In Figs. 12–14 we show, respectively, the avalanche-size distribution and the distribution of $\langle h \rangle$ as a function

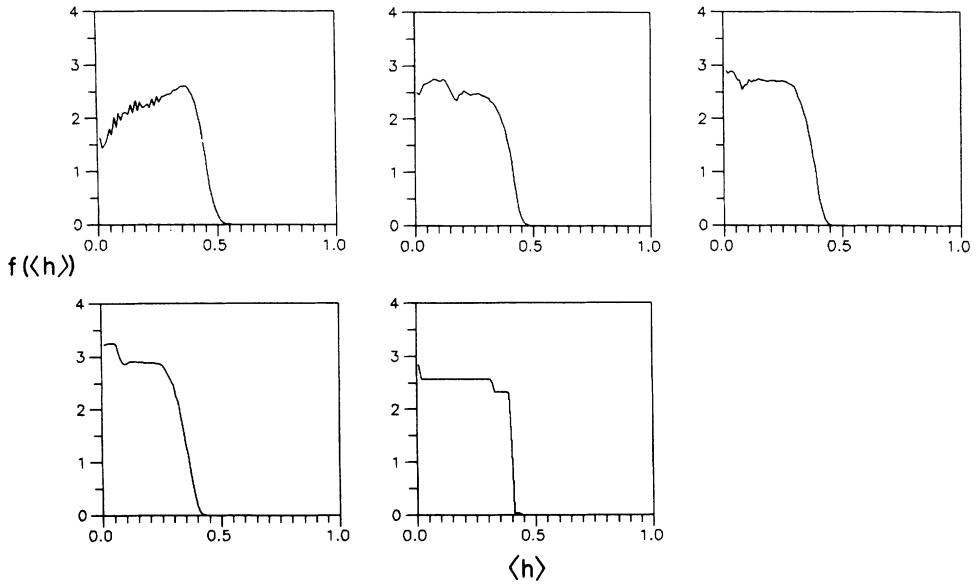

FIG. 13. Relative frequency of occurrence $f(\langle h \rangle)$ of the mean energy $\langle h \rangle$ for model 3.

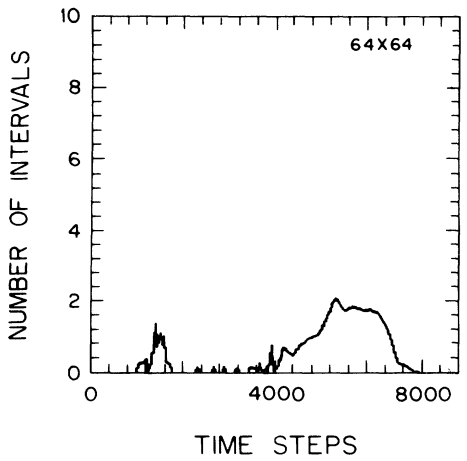

FIG. 14. Distribution of intervals between large events for model 3.

of lattice size, and the time-interval distribution between large events. For this particular model we had to go to larger lattices, with N up to 128, because the trends were not easy to determine for the smaller lattices. With the five lattice sizes under study we see that this model, although conservative, behaves more like model 1 than like model 2: it does not organize into a steady state, and the fracture-size distribution separates into a bimodal distribution which does not span all avalanche sizes. It appears that the question of self-organization into a steady state depends on more than merely having conservative or nonconservative dynamics.

V. ENSEMBLE FRAMEWORK: EPIDEMICS MODEL

We now develop an epidemic [13] growth model for fracture propagation, closely related to the avalanche description of Sec. IV, with a view to understanding the appearance of a power-law decay in the cluster-size distribution of model 2. This model is explicitly constructed to mimic the dominant features of the avalanche dynamics.

Again consider fracture propagation as a process restricted to a discretized plane. At every lattice site (i,j) we have an energy h_{ij}, which we may view as an external field, and allow for a site-dependent nearest-neighbor coupling parameter J_{ij}. The energy values are assumed to be distributed according to a probability distribution $\mathcal{P}(h_{ij})$ which is the result of an ensemble of possible configurations consistent with a set of external constraints. We propose a growth model following the prescription presented by Lomnitz-Adler and Lemus-Diaz [8] for fracture growth on a heterogeneous seismic fault. The basic features of their model which we shall adopt are the following.

(1) Growth is initiated at a seed site chosen at random.

(2) For a given cluster, a growth site is selected on the perimeter, and a number q, which depends on the state of fracture of its neighbors, is assigned to the site.

(3) A probability $p(q)$ that the site fracture is defined.

(4) A random number R, $0<R<1$, is generated; if $R<p$, the site fractures and the cluster grows.

(5) Steps (2)–(4) are iterated until no more growth sites remain.

Step (3) depends on a coupling constant, which in Ref. [8] has a fixed value. We introduce a coupling that depends on the size of the cluster in accordance with the dependence of the stress concentration on fracture size derived in Sec. IV. The connection with the avalanche models can be made as follows: consider a boundary site (i,j) at some point in the evolution of an avalanche, whose energy is

$$h_{ij}=h_{ij}^{0}+J_{ij} , \tag{5.1}$$

where h_{ij}^{0} is the energy of the site prior to the initiation of the avalanche and is the external field in the ensemble approach. The term J_{ij} is the energy transferred by the q broken neighboring sites (coupling constant in the ensemble approach). We make contact at a mean-field level with Eq. (4.4) through the following identification:

$$\langle h\rangle_{\text{perimeter}}=\langle h\rangle+\langle h\rangle(S/t)\equiv\langle h\rangle+\langle q\rangle J(S,t) , \tag{5.2}$$

where $\langle\ \rangle$ denotes an ensemble average defined below, $\langle q\rangle$ is the average number of broken neighbors, and the effective coupling parameter $J(S,t)$ is proportional to the area to perimeter ratio of the crack (cluster).

The mean-field approximation assumes that the energies at different sites are uncorrelated prior to the initiation of growth of the cluster, i.e., their values have a distribution $\mathcal{P}(h)$ which is independent of position. The average energy is now given by

$$\langle h\rangle=\int h\mathcal{P}(h)dh , \tag{5.3}$$

where the integral is taken from zero to infinity in order to allow for the avalanche model 2 situation. Incorporating Eq. (4.5), the effective coupling parameter $J(S)$ is

$$\begin{aligned} &J(S,t)=J(S)=J_0S^{\nu} ,\\ &J_0\simeq\langle h\rangle . \end{aligned} \tag{5.4}$$

Equation (5.4) describes the cluster-size dependence of the coupling parameter consistent with our avalanche models.

It remains to specify the definition of the probability of fracture $p_{ij}(q)$ at a cluster boundary site (i,j). For the avalanche models, we have a threshold dynamics in which the site breaks if $h_{ij}=(h_{ij}^{0}+J_{ij})>1$. We now write $J_{ij}=q_{ij}J$, where J is given by (5.4). In order to mimic the threshold dynamics, we define the probability $p(q)$ that a site on the cluster boundary with q broken neighboring sites breaks by

$$\begin{aligned} &p(q)=\int_{1-Jq}^{\infty}dh\,\mathcal{P}(h)\\ &\int_{0}^{\infty}dh\,\mathcal{P}(h)=1 . \end{aligned} \tag{5.5}$$

Our results do not depend strongly on the specific form of $\mathcal{P}(h)$.

Our growth algorithm is the Leath prescription [14], in which a cluster grows in successive shells, J being the same in each shell, and the sites within each shell are assumed to fracture simultaneously. This is the same algorithm used in the avalanche simulations.

VI. CLUSTER GROWTH PHASE DIAGRAM AND PERCOLATION

In this section we utilize some results from percolation theory to elucidate features of the power-law decay observed in model 2. We show that if $\nu > 0$ and $J_0 > 0$, as in this problem, the system always has a finite probability of percolating, i.e., there is no attainable critical point. This result is established through an interplay between percolation, correlated percolation and this growth model. If $J_0 = 0$ and $\nu = 0$ we have percolation theory [15], while if $J_0 > 0$ and $\nu = 0$ we have a problem of correlated percolation which falls in the same universality class as percolation [16]. In our problem, with $J_0 > 0$ and $\nu > 0$, we are outside the universality class of percolation; however, by making reference to the previous cases, some general properties may be deduced.

In Fig. 15 we show a schematic phase diagram for correlated epidemic models with $\nu = 0$. There is a line of critical points $J_c(\langle h \rangle)$ which separates two regions: one for which the order parameter, the percolation probability $\mathcal{Q}$, is zero, and one for which it is finite. At any point on this line the cluster-size distribution $\rho(S)$ follows the power law $S^{-\tau+1}$ where the exponent τ takes its percolation value of 2.05. In the neighborhood of any of these points, the usual percolation scaling relations hold.

In the case $\nu > 0$ the effective $J(S)$ [Eq. (5.4)] of a growing cluster increases with size following the trajectory indicated by the arrows in Fig. 15. There is a critical cluster size S_c such that

$$J(S_c) = J_0 S_c^{\nu} = J_c(\langle h \rangle, \nu = 0) , \tag{6.1}$$

at which the coupling constant appears to be that of correlated percolation at criticality. For any value of J_0, there is a finite probability of growing a cluster whose size exceeds S_c; further, for any such cluster there is a finite probability of additional growth and percolation.

For a given pair $(\langle h \rangle, J_0)$ the cluster-size distribution can be expected to resemble the schematic diagram of Fig. 16. For cluster sizes in the neighborhood of S_c the coupling constant is approximately equal to that of percolation theory because at S_c, $dJ/dS = J_0 S_c^{-1+\nu}$ is small, and consequently $J(S)$ changes slowly with cluster size. Hence, we expect to find a range of S values for which the cluster-size distribution scales as in percolation theory. Recall that there is a finite probability $\mathcal{Q}$ of growing a percolating cluster of infinite size. If S_c is of the order of the lattice size, $S_c \simeq N^2$, this percolating cluster will appear to be finite and the cluster-size distribution will resemble the dashed curve in Fig. 16. Under these circumstances, from Eqs. (5.2), (5.4), and (6.1), we have that $J_0 N^{2\nu} \simeq \langle h \rangle N^{2\nu} \simeq J_c(\langle h \rangle, \nu = 0)$ from which we recover Eq. (4.6),

$$\langle h \rangle \sim N^{-2\nu} . \tag{6.2}$$

We now interpret the scaling behavior of model 2 as an apparent percolation-class critical behavior due to the finite size of the system. The system self-organizes by tuning its average energy through Eq. (6.2) in order to achieve the critical parameters of the $\nu = 0$ epidemics model near the largest possible fractures.

A quantitative test of this interpretation is an estimate of the slope of the avalanche-size distribution (Fig. 8) in the region near the largest avalanches in terms of percolation theory in the neighborhood of p_c. Let $\rho(S)$ be the correlated percolation cluster-size distribution function. Near the line of critical points of Fig. 15, the cluster-size distribution associated to a set $(\langle h \rangle, J)$ maps onto that of percolation theory for an effective probability p. In the avalanche models we observe fluctuations in the average energy $\langle h \rangle$; variation in the perimeter to surface ratio of the clusters also induces variations in J, which result in a distribution $g(p)$ of probabilities in the associated percolation problem. We write

$$\rho(S) = \int_0^1 g(p) n_S(p) S \, dp , \tag{6.3}$$

where $n_S(p)$ is the number of S clusters per unit site. In-

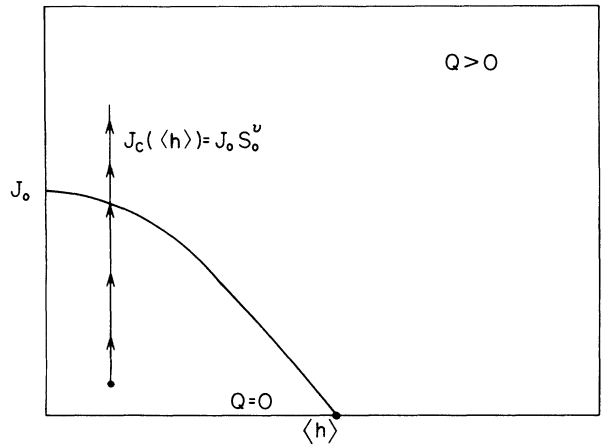

FIG. 15. Schematic phase diagram for correlated epidemics model ($\nu = 0$). The curve is a line of critical points in the percolation universality class. Arrowed line is the trajectory followed during the growth of a cluster in the $\nu > 0$ case.

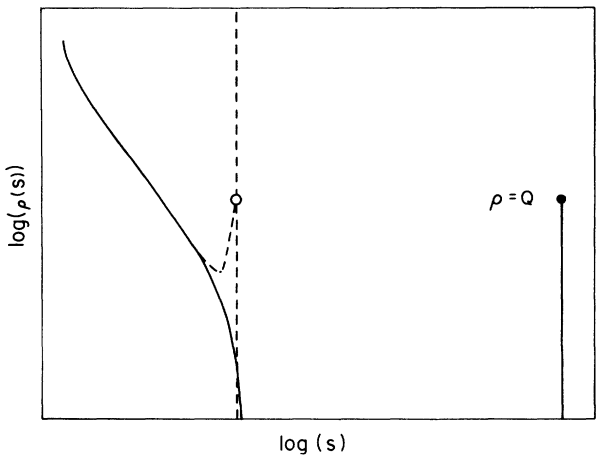

FIG. 16. Schematic diagram of the cluster size distribution for a $\nu > 0$ correlated epidemics model. The cluster at the far right is infinite and occurs with finite probability $\mathcal{Q}$.

troducing the usual percolation-theory scaling expression $n_S(p)=f(z)/S^{\tau}$, with $z=(p-p_c)S^{\sigma}$, into (6.3), we have

$$\rho(S)=S^{-\tau-\sigma+1}\int f(z)[g(p_c)+(z/S^{\sigma})g'(p_c)+\cdots]dz$$
$$\simeq AS^{-\tau-\sigma+1}+BS^{-\tau-2\sigma+1}+\cdots, \quad (6.4)$$

where we have expanded $g(p)$ around p_c and A, B are constants. Substituting the percolation values $\tau=2.05$ and $\sigma=0.4$ in (6.4), the leading term for the cluster-growth-size distribution in our epidemic model should scale with an exponent -1.45. For comparison, we have drawn a straight line with slope -1.45 near the distribution for the largest avalanches in Fig. 8.

VII. DISCUSSION

In this paper we have constructed several nearest-neighbor planar models of seismic shear crack propagation with the property that broken sites are incapable of accumulating energy for the duration of the fracture. The models differ only according to the rule that must be invoked for the seemingly rare case in which the energy of a site exceeds the threshold for rupture, and yet has no nearest neighbors to which this energy can be transferred because they are all broken sites. In the first model the energy was transferred directly out of the system; in the second, the site did not rupture until some later fracture event, and in the third, the site ruptured and its energy was transferred to the entire crack perimeter. The first and third models generate bimodal fracture distribution functions; model 2 generates fractures of all sizes which satisfy a power-law distribution except for fractures whose size are almost those of the lattice itself.

Our results can be understood in terms of a classical nucleation process, provided that in model 2 the perimeter is allowed to scale in a not-trivial way with cluster size. The scaling behavior observed in model 2 is a consequence of an unusual form of self-organization. The system tunes itself into a steady state for which the critical cluster size, i.e., the largest avalanche which does not result in mechanical instability, is comparable to the lattice dimensions. This tuning is manifested in the size dependence of the system's mean energy.

The power laws generated by the model can be understood, via an epidemic model, in terms of finite-size effects and percolation theory. In most systems which exhibit critical behavior, finite size tends to soften the singularities, in this case they produce an *apparent* second-order phase-transition behavior of the percolation universality class. The avalanche-size distribution has a power-law decay that is very close to that expected from percolation theory (see Fig. 8), while the exponent $\nu\cong 0.25$ in the perimeter to area ratio $t/S\sim S^{-\nu}$ obtained from Fig. 9, is incompatible with the percolation value $\nu_{\text{perc}}=0$. This can be understood if we accept that, although the system does not belong to the universality class of percolation, the largest finite cracks grow in a manner analogous to an epidemic model of the percolation class near the critical point. It is in fact the nonzero ν which drives the system towards a pseudocritical point, providing a mechanism of dynamic selection. Other mechanisms capable of such a selection appear in invasion percolation [17] and the two-state models of Carlson *et al.* [18]. In model 2, as in [18], finite-size effects play a central role in generating the observed "critical" behavior. In our case even the location of the critical region is size dependent.

While universal agreement as to what constitutes self-organized criticality does not exist, one of the signatures of this phenomenon is considered to be the appearance of power laws and scaling relations. Although our models share some features in common with previous automaton models, the principal differences are that all three of our models preserve a memory of rupture for the duration of a fracture, i.e., healing of the frictional bonds in the fracture takes place only after the entire fracture has been completed, whereas in Bak, Tang, and Wiesenfeld [2] and Zhang [3] all sites have exactly the same properties whether they have ruptured or not. For this reason we describe our models as being temporally nonlocal. Model 1 is not conservative. Model 2 is conservative and all energy transfers are between nearest neighbors. Model 3 is conservative but is not spatially local. Our results are summarized in Table I.

Hwa and Kardar [12] state that a necessary condition for a system to self-organize into a critical state is that it be conservative. Model 3, while being conservative, does not settle into a steady state, indicating the relevance of locality. It is tempting to think that a conservative local dynamics is a sufficient condition for SOC. However model 2, though capable of generating power-law decays, does not sit at a critical point. This fact is brought out when the tail of the size distribution is considered: there is a large probability of generating avalanches whose size is comparable to the lattice dimensions themselves and which do not allow for a simple finite-size scaling analysis. We conjecture that such spikes in the avalanche-size distribution function can be used as a signature to distinguish between avalanche dynamics which are analogous to systems with first-order phase transitions and systems at criticality. All of our models present behavior reminiscent of first-order phase transitions and, we believe, the same applies to the Burridge-Knopoff [19] nonconservative model with nearest-neighbor dynamics studied in detail by Carlson and Langer [5]. Though the question of what is a sufficient condition for SOC remains open, much effort is currently being applied in this direction [18].

Avalanche models such as these have been proposed to describe earthquake dynamics [4,5,6,20], the principal at-

TABLE I. Dependence of self-organized criticality on general features of the models. Zhang's results are those of Ref. [3]. For more details see text.

Model	Local	Memory	Conservative	SOC
Zhang	Yes	No	Yes	Yes
1	Yes	Yes	No	No
2	Yes	Yes	Yes	"Yes"
3	No	Yes	Yes	No

traction being that by such means one can generate the well-known Gutenberg-Richter relation which is a power law in the frequency of occurrence of earthquakes of a given moment. With respect to the models discussed in this paper, models 1 and 3 generate bimodal size-frequency relations, the first branch being an approximate power law which is cut off at a critical size. We have found that as the surface roughness is increased, this power-law region extends to larger avalanche sizes. Model 2 is nonphysical, yet has the property that it is capable of generating its own surface roughness. This model can generate power-law size distributions which extend to the very largest avalanches which the system can support. We conclude from these results that avalanche models of the kind presented in this paper can reproduce the Gutenberg-Richter relation provided that the energy surface is allowed to be sufficiently rough. We also note that a discrepancy between our model and earthquake distributions is that, while it is a popular seismological assumption that all earthquake events are members of a single population, in the model distributions two distinct populations can be identified. Since the largest model events are dissipative, we may speculate that an improvement in the application of models of this type to earthquake problems will take place after a closer analysis of dissipation [21] and the influence of the boundary conditions [22].

One system to which models of this class could apply is the sandpile that inspired the original work on SOC. Jaeger, Lin, and Nagel [23] found that the avalanches obtained in real sandpiles generate a bimodal distribution, and that the average slope lies between two angles of instability Θ_m and repose Θ_r. Based on models 1 and 3, we expect the experimental determination of Θ_m to yield different values for those experiments carried out by tilting the sandpile slowly as in Ref. [19] where $\Theta_m \rightarrow h = 1$, and those where grains are deposited randomly and $\Theta \rightarrow \langle h \rangle_{\rm tr} = 0.4$. The finite-size effects discussed in Ref. [24] can be understood within the context of model 1 if the small sandpiles studied in Ref. [25] are smaller than the critical avalanche size L_c, so that all avalanches lie within the scaling region.

ACKNOWLEDGMENTS

Much of this work was done while J. Lomnitz-Adler was a recipient of financial support from the John Simon Guggenheim Memorial Foundation, to which he expresses his gratitude. J. L-A and G. M-M acknowledge support from DGAPA-UNAM Grant No. IN105089.

[1] J. H. Dieterich, Pure Appl. Geophys. **116**, 790 (1978); J. Geophys. Res. **84**, 2161 (1979).
[2] P. Bak, C. Tang, and K. Wiesenfeld, Phys. Rev. Lett. **59**, 381 (1987) Phys. Rev. A **38**, 364 (1988).
[3] Y.-C. Zhang, Phys. Rev. Lett. **63**, 470 (1989).
[4] K. Ito and M. Matsuzaki, J. Geophys. Res. **95**, 6853 (1990).
[5] J. M. Carlson and J. S. Langer, Phys. Rev. Lett. **62**, 2632 (1989); Phys. Rev. A **40**, 6470 (1989).
[6] N. Nakanishi, Phys. Rev. A **41**, 7086 (1990).
[7] See, for example, *Statistical Models for the Fracture of Disordered Media,* edited by H. J. Herrmann and S. Roux (North-Holland, Amsterdam, 1990).
[8] J. Lomnitz-Adler and P. Lemus-Diaz, Geophys. J. Int. **99**, 183 (1989).
[9] B. V. Kostrov and S. Das, *Principles of Earthquake Source Mechanics* (Cambridge University Press, Cambridge, England, 1988); J. R. Rice, in *The Mechanics of Earthquake Rupture,* Proceedings of the International School of Physics "Enrico Fermi" Course LXXVIII, Varenna, 1979, edited by A. M Dziewonski and E. Boschi (North-Holland, Amsterdam, 1980), p. 555.
[10] L. Knopoff, Geophys. J. R. Astron. Soc. **1**, 44 (1958).
[11] L. P. Kadanoff, S. R. Nagel, L. Wu, and S. Zhou, Phys. Rev. A **39**, 6524 (1989).
[12] T. Hwa and M. Kardar, Phys. Rev. Lett. **62**, 1813 (1989).
[13] H. J. Herrmann, Phys. Rep. **136**, 153 (1986).
[14] P. L. Leath, Phys. Rev. B **4**, 5046 (1976).
[15] D. Stauffer, Phys. Rep. **54**, 1 (1979); J. M. Essam, Rep. Prog. Phys. **43**, 839 (1980).
[16] A. Bunde, H. J. Herrmann, A. Margolina, and H. E. Stanley, Phys. Rev. Lett. **55**, 653 (1985); M. Napiorkowski and P. C. Hemmer, Phys. Lett. **76A**, 359 (1980).
[17] D. Wilkinson and J. F. Willemsen, J. Phys. A **16**, 3365 (1983).
[18] J. M. Carlson, J. T. Chayes, E. R. Swindle, and G. H. Swindle, Phys. Rev. A **42**, 2467 (1990).
[19] R. Burridge and L. Knopoff, Bull. Seismol. Soc. Am. **57**, 341 (1967).
[20] A. Sornette and D. Sornette, Europhys. Lett. **9**, 197 (1989).
[21] J. Lomnitz-Adler (unpublished).
[22] L. Knopoff and J. A. Landoni (unpublished).
[23] H. M. Jaeger, C. H. Liu, and S. R. Nagel, Phys. Rev. Lett. **62**, 40 (1989).
[24] C. H. Liu, H. M. Jaeger, and S. R. Nagel, Phys. Rev. A **43**, 7091 (1991).
[25] G. A. Held, D. H. Solina II, D. T. Keane, W. J. Haag, P. M. Horn, and G. Grinstein, Phys Rev. Lett. **65**, 1120 (1990).